JACS
JOURNAL OF THE AMERICAN CHEMICAL SOCIETY
Article
pubs.acs.org/JACS

Controlling Chemical Self-Assembly by Solvent-Dependent Dynamics

Peter A. Korevaar, Charley Schaefer, Tom F. A. de Greef,* and E. W. Meijer*

Institute for Complex Molecular Systems and Laboratory of Macromolecular and Organic Chemistry, Eindhoven University of Technology, P.O. Box 513, 5600 MB, Eindhoven, The Netherlands

Supporting Information

ABSTRACT: The influence of the ratio between poor and good solvent on the stability and dynamics of supramolecular polymers is studied via a combination of experiments and simulations. Step-wise addition of good solvent to supramolecular polymers assembled via a cooperative (nucleated) growth mechanism results in complete disassembly at a critical good/poor solvent ratio. In contrast, gradual disassembly profiles upon addition of good solvent are observed for isodesmic (non-nucleated) systems. Due to the weak association of good solvent molecules to monomers, the solvent-dependent aggregate stability can be described by a linear free-energy relationship. With respect to dynamics, the depolymerization of π-conjugated oligo(*p*-phenylene vinylene) (OPV) assemblies in methylcyclohexane (MCH) upon addition of chloroform as a good solvent is shown to proceed with a minimum rate around a critical chloroform/MCH solvent ratio. This minimum disassembly rate bears an intriguing resemblance to phenomena observed in protein unfolding, where minimum rates are observed at the thermodynamic midpoint of a protein denaturation experiment. A kinetic nucleation−elongation model in which the rate constants explicitly depend on the good solvent fraction is developed to rationalize the kinetic traces and further extend the insights by simulation. It is shown that cooperativity, i.e., the nucleation of new aggregates, plays a key role in the minimum polymerization and depolymerization rate at the critical solvent composition. Importantly, this shows that the mixing protocol by which one-dimensional aggregates are prepared via solution-based processing using good/poor solvent mixtures is of major influence on self-assembly dynamics.

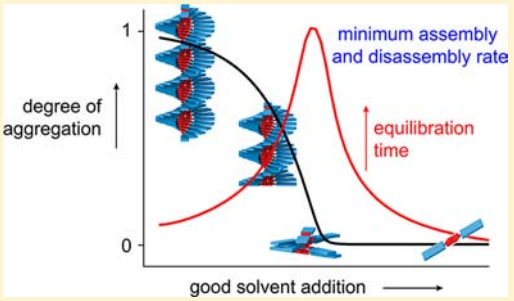

1. INTRODUCTION

Self-assembly of small molecules offers a practical approach to build molecular nanostructures.[1] Self-assembled one-dimensional[2] nanomaterials consisting of organic molecules are particularly attractive with applications ranging from nanoelectronics[3] to biomaterials[4] designed for cell scaffolding.[5] To control the supramolecular organization of self-assembled materials, a prerequisite for the optimal performance, an in-depth understanding of the processing methodology is of utmost importance. Often, processing starts from a good solvent in which the building blocks are molecularly dissolved. Subsequently, self-assembly is induced by transfer of the molecules to a poor solvent which induces aggregation.[6] As a consequence, the selected solvent conditions play a key role in the self-assembly process: the stability of the aggregated structures[7] and even the morphology[6b,8] can be controlled by tuning the ratio between good and poor solvent.

Recently, it is shown that the formation of self-assembled structures can be affected by metastable, off-pathway aggregates that compete with the thermodynamically stable state for free monomers and thereby exert their influence on the rate of the overall assembly process.[9] These insights emphasize the importance of control over assembly pathways, both in terms of stability as well as dynamics. For this reason, different processing methodologies are applied in self-assembly processes that are induced by a transfer from good to poor solvent, varying from fast dispersion to (slow) vapor diffusion.[6a] However, although a start has been made to control the subtleties in self-assembly processes by tuning the solvent conditions, more detailed insight is needed to arrive at optimized nanoscopically ordered materials.

The role of solvent in the control over noncovalent interactions has been studied for decades in protein folding.[10] It is for example well-known that proteins can unfold—or denaturate—by the addition of urea. The denaturation process in case of simple peptides is often described as a two-state equilibrium between a folded (F) and an unfolded (U) state. Due to the linear dependence of the Gibbs free energy of folding on the denaturant concentration, addition of a denaturant results in a gradual destabilization of the folded state.[11] Remarkably, the unfolding as well as the folding processes have a minimum rate at the denaturant concentration corresponding to the thermodynamic midpoint of the denaturation curve, which results in characteristic "chevron plots".[12] This phenomenon can be rationalized by assuming that the rate constant of folding decreases upon adding denaturant, whereas the rate constant of unfolding increases with denaturant. Consequently, the overall

Received: June 7, 2012
Published: July 18, 2012

   dx.doi.org/10.1021/ja305512g | *J. Am. Chem. Soc.* 2012, 134, 13482−13491

Chart 1. Molecular Structures of Self-Assembling Moieties 1−4

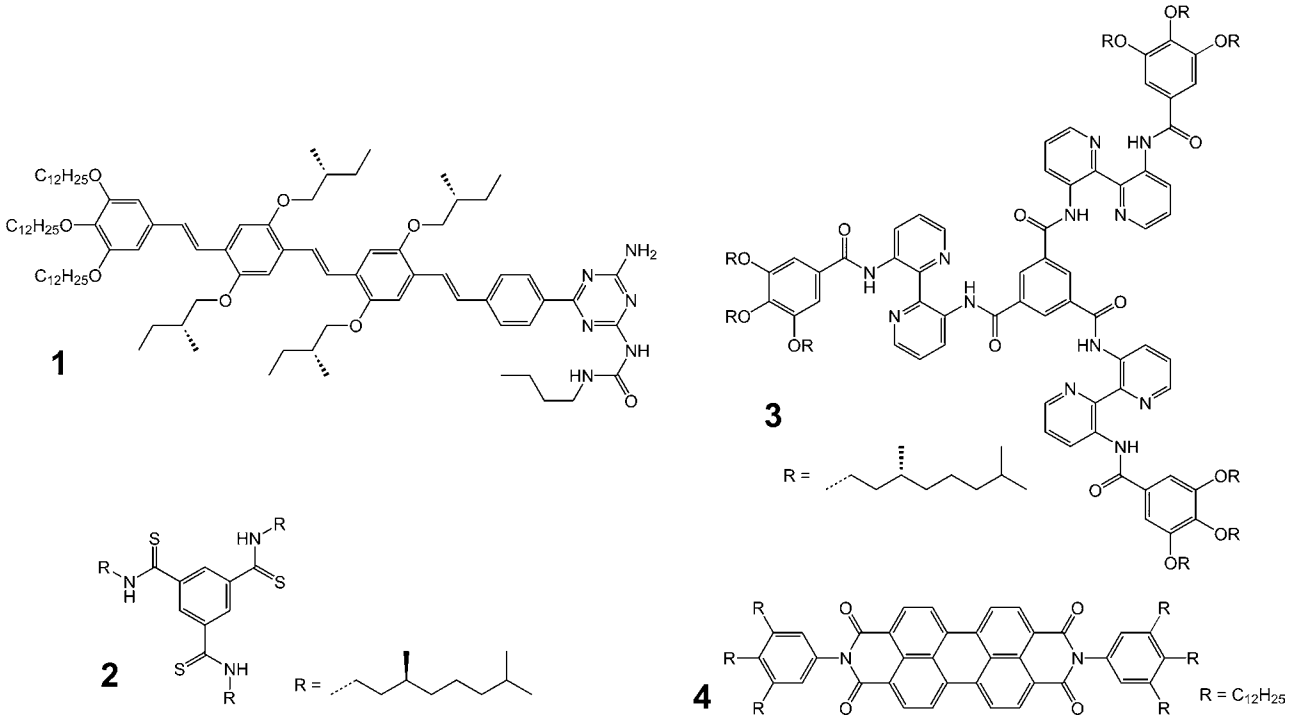

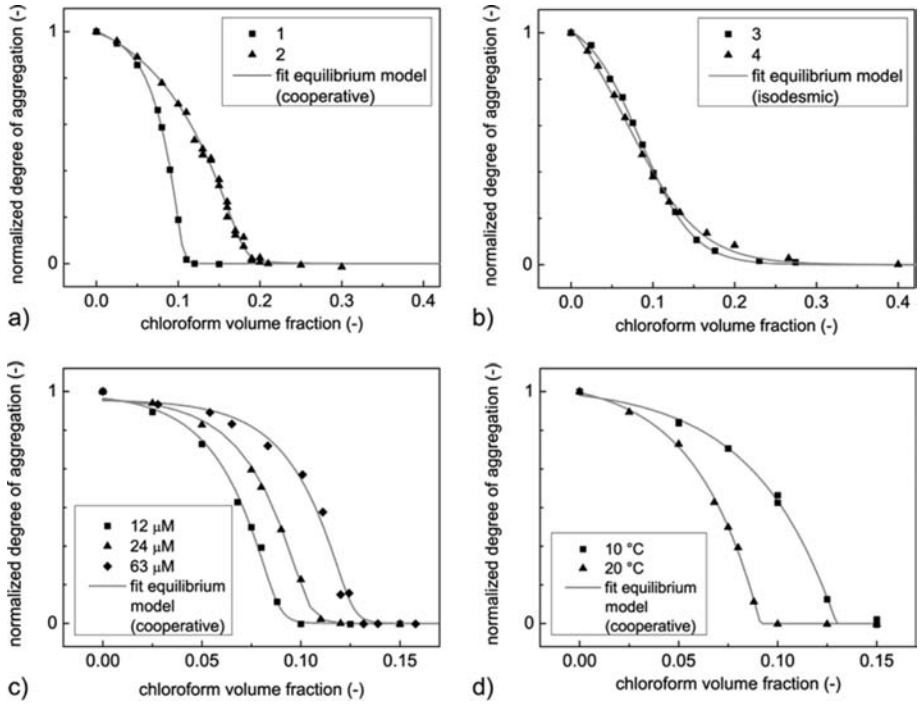

Figure 1. Disassembly of supramolecular polymers induced by increasing the ratio of good solvent chloroform starting from poor solvent MCH. The denaturation curves of both cooperative (nucleated) supramolecular polymers (a, **1** and **2**) as well as isodesmic (non-nucleated) supramolecular polymers (b, **3** and **4**) are fitted with the equilibrium model which includes a Gibbs free energy of monomer association that is linearly dependent on the chloroform volume fraction (20 °C; **1**, 24 μM; **2**, 19 μM; **3**, 14 μM; **4**, 146 μM). The critical chloroform volume fraction at which the supramolecular polymer of **1** is fully disassembled is found to increase with concentration (c, 20 °C) and decrease with temperature (d, 12 μM), in agreement with the equilibrium model.

observed relaxation rate shows a V-shaped dependence on the denaturant concentration, with a minimum at the midpoint of the denaturation equilibrium curve.

The insights developed in the field of protein folding prompted us to investigate how the influence of solvent conditions on supramolecular polymerization can be rationalized, both in terms of stability (thermodynamics) and dynamics (kinetics). In the first part of this paper a clear relation is shown between the assembly mechanism and the stability of the aggregates upon addition of good solvent. Supramolecular

dx.doi.org/10.1021/ja305512g | J. Am. Chem. Soc. 2012, 134, 13482−13491

polymers assembled via a cooperative (nucleated) growth mechanism are demonstrated to disassemble completely at a critical good/poor solvent ratio. In the second part, we show that the disassembly of a π-conjugated nanofiber based on an oligo(*p*-phenylene vinylene) (OPV) proceeds with the slowest dynamics close to this critical solvent composition. This phenomenon bears an intriguing resemblance to denaturant-dependent rate effects observed in protein unfolding. In the third part, we show and rationalize how the mixing protocol influences the development of the self-assembled system in time after addition of good solvent. Finally, a qualitative dynamic model is developed to describe the polymerization and depolymerization process by sequential monomer addition and dissociation. The theoretical model qualitatively captures the essential experimental results and furthermore enables us to expand the insights by simulations.

2. RESULTS AND DISCUSSION

2.1. Thermodynamic Relation between Solvent Composition and Stability of Self-Assembled Structures. The assembly of *R*-chiral oligo(*p*-phenylene vinylene)-ureidotriazine[13] (OPV) **1**, *S*-chiral benzene-1,3,5-trithioamide[14] **2**, *R*-chiral 3,3′-diamino-2,2′-bipyridine C_3-discotic[15] **3**, and perylene tetracarboxylic acid bisimide[16] **4** (Chart 1) are probed with circular dichroism (CD, **1**−**3**) and UV−vis spectroscopy (**4**), respectively. These monomers self-assemble in methylcylohexane (MCH), whereas their molecularly dissolved states can be obtained in pure chloroform. In analogy to protein denaturation studies, the self-assembly is studied in different solvent mixtures of poor (MCH) and good (chloroform) solvent (Figure S1, Supporting Information). Since each of these moieties displays a clear transition in CD and/or UV−vis upon aggregation, the degree of aggregation can be deduced from the normalized changes in CD or UV−vis under equilibrium conditions. The degree of aggregation vs chloroform volume fraction (f) reveals a critical solvent composition for the self-assembly of **1** and **2**, whereas a gradual "denaturation" curve is observed for **3** and **4** (Figure 1a,b). The occurrence of a critical solvent composition holds a similarity with the critical temperature of aggregation, typically attributed to a nucleation phenomenon involved in the aggregation process.[17] Indeed, temperature-dependent studies reveal a cooperative aggregation mechanism for **1** and **2**, whereas isodesmic growth is observed for **3** and **4** (Figure S2, Supporting Information).[16,18,19] For **1**, the degree of aggregation vs f is determined at different temperatures and concentrations (Figure 1c,d). The critical chloroform volume fraction (f_{crit}) increases with concentration and decreases with temperature.

To further rationalize the effect of solvent composition on the self-assembly, we analyze the data by expanding the general nucleation−elongation model as first analyzed by Goldstein and Stryer (Supporting Information).[20] In this equilibrium model, the assembly process is described as a sequence of monomer addition equilibria with equilibrium constant K_e. In the case of cooperative growth, the monomer addition steps in the nucleation regime (up to nucleus size n) are described by equilibrium constant K_n, with cooperativity parameter $\sigma = K_n/K_e < 1$. The equilibrium constant K_e is defined via $K_e = \exp(-\Delta G^{0\prime}/RT)$, with $\Delta G^{0\prime}$ being the Gibbs free energy gain upon monomer addition, R the gas constant, and T the temperature. In an analogy with protein denaturation models, the Gibbs free energy is assumed to be linearly dependent on the volume fraction of chloroform:

$$\Delta G^{0\prime} = \Delta G^0 + m \cdot f \quad (1)$$

where ΔG^0 represents the Gibbs free energy gain upon monomer addition in pure MCH and the dependence of $\Delta G^{0\prime}$ on f is described by the m-value. The cooperativity parameter σ is assumed to be independent of f (i.e., the m-value involved in the nucleation Gibbs free energy equals the m-value involved in further growth).

Simulations with the equilibrium model reveal a critical solvent composition below which cooperative growth of a supramolecular polymer ($\sigma < 1$) occurs, whereas a gradual denaturation curve is obtained in case of an isodesmic growth mechanism ($\sigma = 1$). Furthermore, the position of the critical solvent composition is found to increase with the stability of the aggregate in pure MCH (proportional to the free energy release upon monomer addition, $-\Delta G^0$) and with the total monomer concentration, as is also observed experimentally (Figure S3, Supporting Information).

Curve fitting by applying a global nonlinear least-squares procedure using the equilibrium model gives a very good description of the data for both supramolecular polymers growing via a cooperative (**1** and **2**) as well as an isodesmic (**3** and **4**) mechanism (Figure 1a,b). As shown in Table 1 and the Supporting Information, multiple curve fitting of denaturation curves acquired at different concentrations of **1** allows an accurate and uncorrelated determination of the parameters, the obtained values of ΔG^0 and σ are in good agreement with temperature-dependent analysis. As in the curve fitting procedure multiple denaturation curves obtained at different total concentrations of **1** are used, it can be concluded that the m-value that describes the decrease in stability of the aggregated state is independent of the total monomer concentration (Figure 1c).

Table 1. Results of Multiple Curve Fitting of Denaturation Curves of 1 with the Equilibrium Model

ΔG^0 (kJ/mol)	m (kJ/mol)	σ
−39.9 ± 0.4	109 ± 3	0.25 ± 0.04

In protein denaturation studies, a linear decrease of the Gibbs free energy of folding upon addition of denaturant is rationalized by the weak association of many denaturant molecules to the polyamide backbone which competes with the hydrogen-bond formation involved in the protein folding itself.[21] As a consequence of the manifold of weak interactions of the denaturant molecules to one amide group, the resulting stability of the folded state can be described via a linear Gibbs free energy relation rather than taking into account all the denaturant association equilibria. Interestingly, detailed investigations by Moore and co-workers revealed a similar phenomenon in the folding of synthetic foldamers, in which the weak association of chloroform to the π-conjugated units of a foldamer results in a linear relation between Gibbs free energy of folding and chloroform concentration.[22] Our results show that this behavior is not limited to the intramolecular folding of proteins or synthetic foldamers but is more general and can also be observed in supramolecular systems with molecular components assembling via intermolecular association.

Traditionally, self-assembly mechanisms are often identified via concentration- or temperature-dependent studies.[17a] However, the concentration-dependent transition from the monomeric to the fully aggregated state typically covers three

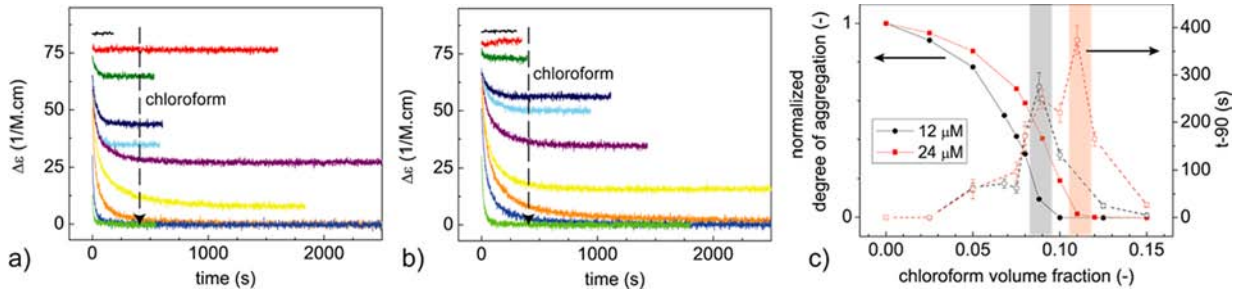

Figure 2. The depolymerization of OPV in MCH induced by addition of OPV in chloroform is followed in molar ellipticity ($\Delta\varepsilon$) vs time for different chloroform volume fractions. The experiments are performed at an OPV concentration of (a) 12 and (b) 24 μM at 20 °C. (c) The normalized degree of aggregation vs chloroform volume fraction is derived from the steady-state CD intensities in the kinetic experiments. For both concentrations, the time at which 90% of the conversion toward the equilibrium state is obtained (t-90) vs chloroform volume fraction shows a maximum close to the critical chloroform volume fraction at which just enough chloroform is added to induce full disassembly.

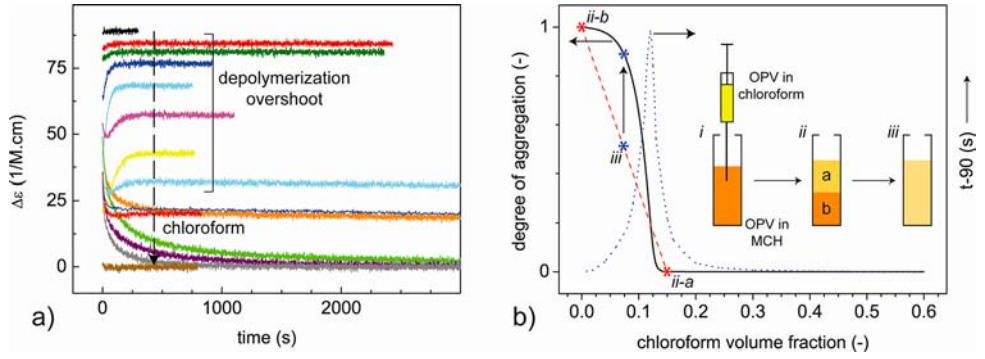

Figure 3. (a) Depolymerization kinetics of OPV in MCH, induced by addition of OPV in chloroform at high concentration (63 μM, 20 °C). (b) The depolymerization overshoot can be rationalized by inefficient mixing in the initial stages of the depolymerization experiment. To illustrate this, we consider the mixing of OPV in MCH with OPV in chloroform, aiming for $f = 0.075$ (*i*). Due to insufficient mixing however, initially in the upper half of the cuvette f equals 0.15 (*ii-a*), whereas in the lower half of the cuvette f equals 0 (*ii-b*). As a consequence, rapid depolymerization is obtained in *ii-a*, whereas no depolymerization takes place in *ii-b*. Subsequently, further mixing results in a homogeneous mixture (*iii*, $f = 0.075$), with an average degree of aggregation on the red dashed line. However, the equilibrium average degree of aggregation at $f = 0.075$ (0.90) is larger than the degree of aggregation obtained after mixing (0.50), resulting in reassembly.

(cooperative) to four (isodesmic) orders of magnitude in concentration.[17] Such an extended concentration window often exceeds the limits of an experimental technique. Furthermore, temperature-dependent studies can be hampered by solubility, stability, or lower critical solution temperature (LCST) issues as well. Our denaturation studies on **1** and **2** show that cooperative supramolecular polymerizations display a critical solvent composition: an easily recognizable characteristic to distinguish between cooperative and isodesmic growth. Hence, denaturation studies provide the chemist with an alternative methodology to unravel self-assembly pathways involved in systems that cannot be studied by concentration- or temperature-dependent studies. Moreover, the influence of solvent composition on the stability of a supramolecular polymer plays an important role in the dynamics of cooperative systems, as shown in the next part of this paper.

2.2. Kinetic Studies on Depolymerization by Cosolvent Addition. The depolymerization kinetics of **1** are studied by manually mixing a solution of molecularly dissolved OPV in chloroform (12 μM) with a solution of OPV assemblies in MCH (12 μM) in different ratios. The chloroform-induced disappearance of the helical OPV assemblies in time is followed by probing the CD effect at 466 nm (Figure 2a). Intriguingly, the rate, characterized by the time at which 90% of the conversion toward the equilibrium state is obtained (t-90), shows a minimum close to the critical chloroform volume fraction, as obtained from the equilibrium denaturation curves (i.e., f_{crit}, Figure 2c). In a similar experiment performed at a higher total concentration of **1** (24 μM), the chloroform volume fraction at which the slowest depolymerization is observed again coincides with the critical chloroform volume fraction obtained from the thermodynamic denaturation curve, albeit its value is higher (Figure 2b,c).

2.3. Influence of Mixing Protocol on Self-Assembly Kinetics. To further investigate the depolymerization kinetics, we perform a manual mixing experiment at a higher total concentration of **1** (63 μM, Figure 3a). Again, the depolymerization kinetics are slowest at the critical chloroform volume fraction. However, depolymerization experiments with chloroform volume fractions below 12% show an increasing CD intensity in time. Apparently, directly after mixing of the MCH and chloroform solutions, an overshoot in the depolymerization occurs, and subsequently the system reassembles back to the equilibrium state.

The depolymerization overshoot can be rationalized by the influence of inefficient mixing in the initial stages of the experiment. Imagine a mixing experiment that aims for a homogeneous mixture of 7.5 v/v% chloroform in MCH (Figure 3b). The experiment is performed such that halfway in the mixing procedure, the upper half of the cuvette contains 15 v/v% chloroform, whereas the lower half contains 0 v/v% chloroform. Since the chloroform volume fraction in the top part exceeds f_{crit} (12.5 v/v%), aggregated material in the upper half of the cuvette depolymerizes quickly, whereas no depolymerization takes place in the lower half of the cuvette. Further mixing results in a

dx.doi.org/10.1021/ja305512g | J. Am. Chem. Soc. 2012, 134, 13482−13491

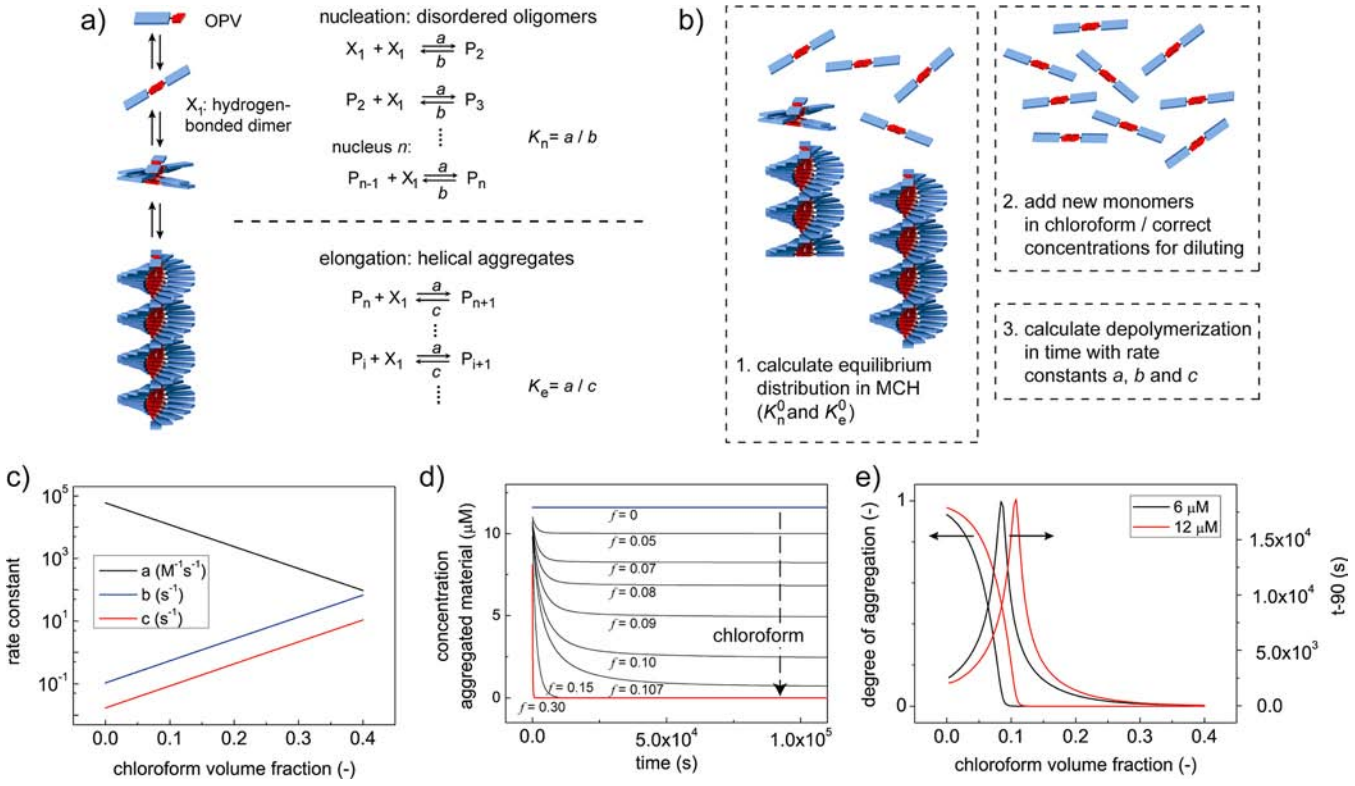

Figure 4. (a) Kinetic nucleation–elongation model to simulate depolymerization of OPV assemblies, in which the hydrogen-bonded OPV dimer (X_1) is considered as the monomer. (b) Schematic representation of followed approach to simulate depolymerization kinetics: (1) The equilibrium distribution of all species with different stack lengths (i = 1, 2, etc.) in pure MCH is calculated via the equilibrium model, using K_n^0 and K_e^0. (2) New monomers that originate from the chloroform phase are added to the monomers present in the MCH solution, and the resulting monomer concentration as well as the concentrations of all aggregate species are corrected for dilution due to mixing of the MCH and chloroform phases. (3) Using these concentrations as start conditions, the subsequent depolymerization kinetics are simulated using the rate constants a, b, and c with values in accordance with the chloroform/MCH ratio. (c) Relation between rate constants a, b, and c and chloroform volume fraction in MCH (based on eqs 2–4, $a^0 = 6 \times 10^4$ $M^{-1}s^{-1}$, $c^0 = 1.71 \times 10^{-2}$ s^{-1}, $m_a = 7$, $m_c = 7$, $\sigma = 0.16$). (d) Simulated depolymerization kinetics with increasing amounts of chloroform (OPV dimer concentration 12 μM, $n = 5$). (e) The time at which 90% of the conversion toward the equilibrium state is obtained (t-90) shows a minimum rate close to the critical chloroform volume fraction.

homogeneous system with 7.5 v/v% chloroform and containing 50% of the assemblies present in the MCH solution before the addition of the chloroform solution (i.e., the average of complete depolymerization in one-half of the cuvette and no depolymerization in the other half). As a result, after complete mixing, the degree of aggregation equals 50% of the degree of aggregation in pure MCH (0.5). However, the degree of aggregation under equilibrium conditions at f = 0.075 equals 0.9, resulting in a reassembly in time.[23]

Although in reality the experiment does not occur via a two step mixing protocol, this thought experiment clearly demonstrates the influence of the mixing efficiency on the depolymerization dynamics of supramolecular polymers. Gratifying, no overshoot in the depolymerization kinetics is observed when the depolymerization experiments are performed in a stopped-flow setup that enables very fast and efficient mixing using a Berger ball mixer. The stopped-flow experiments, at 12 and 51 μM, result in the slowest depolymerization rates close to the critical chloroform volume fraction obtained from the thermodynamic denaturation curves, in agreement with experiments performed using manual mixing at lower concentrations (Figures S8 and S9, Supporting Information).

2.4. Unraveling and Simulating the Influence of Solvent Composition on Supramolecular Polymerization Dynamics via a Kinetic Model. The minimum rate encountered in the depolymerization of OPV assemblies close to f_{crit} holds an intriguing resemblance to protein unfolding dynamics, where a minimum rate is observed at the thermodynamic midpoint of the denaturation curve. In protein unfolding, this phenomenon is rationalized by explicitly taking into account the effect of the denaturant concentration [denaturant] on the rate constants of folding (k_F) and unfolding (k_U) using the relation $\log(k_F) = \log(k_F^0) - m_F \cdot$[denaturant] and $\log(k_U) = \log(k_U^0) + m_U \cdot$[denaturant], with k_U^0 and k_F^0 the rate constants in pure water.[12] In analogy, we extend our previously introduced cooperative supramolecular polymerization kinetic model[9,24] to allow for solvent-dependent rate constants. In this model, prenucleus oligomers (aggregates below the critical nucleus size n) and helical aggregates change size through monomer association and dissociation (Figure 4a). Monomer association to both prenucleus oligomers and helical aggregates is described with forward rate constant a. Monomer dissociation from prenucleus oligomers and helical aggregates is described with backward rate constants b and c, respectively. Under equilibrium conditions, the system can be described by nucleation and elongation equilibrium constants $K_n = a/b$ and $K_e = a/c$. The solvent dependency of the forward and backward rate constants a and c is defined via

$$\log(a) = \log(a^0) - m_a \cdot f \quad (2)$$

dx.doi.org/10.1021/ja305512g | J. Am. Chem. Soc. 2012, 134, 13482–13491

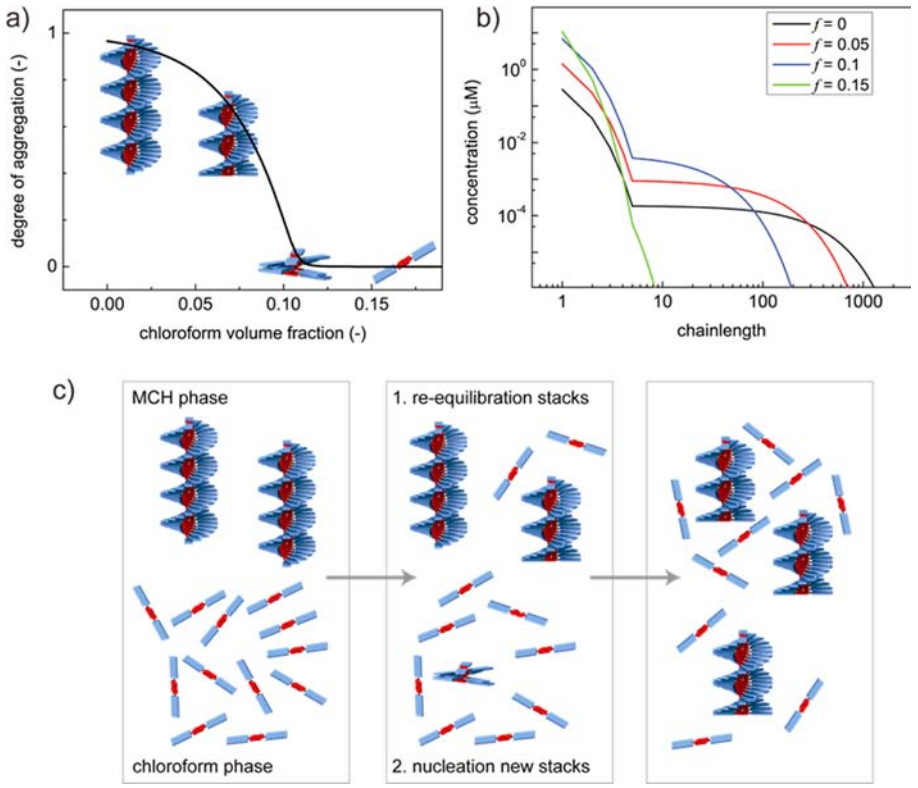

Figure 5. (a) Degree of aggregation vs chloroform volume fraction calculated under equilibrium conditions (K_e^0 = 3.5 × 10^6 M^{-1}, OPV dimer concentration = 12 μM, m = 7.9 × 10^4 J/mol, n = 5, σ = 0.16). (b) For different points on the denaturation curve, the equilibrium distribution (concentration vs chain length) is calculated via the equilibrium model. (c) Schematic representation of development of supramolecular polymer in time after mixing the MCH and chloroform phase: both the long stacks as well as the new monomers re-equilibrate toward the new equilibrium state via depolymerization and nucleation of new stacks, respectively.

$$\log(c) = \log(c^0) + m_c \cdot f \quad (3)$$

respectively, with a^0 and c^0 the rate constants in pure MCH. Rate constant b is defined via

$$b = c/\sigma \quad (4)$$

with cooperativity parameter σ. Equilibrium constants of nucleation K_n^0 and elongation K_e^0 in pure MCH are defined via $K_e^0 = a^0/c^0$ and $K_n^0 = \sigma \cdot K_e^0$. Again, σ is assumed to be independent of f.

To simulate the depolymerization kinetics induced by the addition of OPV in chloroform to the solution of OPV assemblies in MCH, first the concentrations of all oligomers and helical aggregates in pure MCH are calculated via the equilibrium model using realistic values of K_n^0 and K_e^0 (Figure 4b). Subsequently, starting concentrations for the dynamic simulations are obtained by addition of fresh monomers to the monomer pool in MCH and correcting the resulting monomer concentration as well as the concentrations of all aggregate species for dilution due to mixing of the MCH and chloroform phases. Thereafter, the depolymerization kinetics at the respective chloroform/MCH ratio are simulated using these start concentrations together with the rate constants a, b, and c, defined via eqs 2−4 (Figure 4c). The value of the forward rate constant a^0 (i.e., in pure MCH) was chosen close to the value found in previous kinetic studies on OPV self-assembly.[9] The values of the backward rate constant c^0 (which equals a^0/K_e^0), m_a, m_c, and σ were chosen so as to match the experimental melting and denaturation curves obtained under thermodynamic control. Indeed, simulations of the depolymerization dynamics performed at different chloroform volume fractions reveal a minimum depolymerization rate around f_{crit}, as is observed experimentally (Figure 4d,e). However, the simulated maximum values of t-90 at both OPV concentrations are approximately 2 orders of magnitude larger than the experimentally observed values. This difference can be explained by the fact that the kinetic model describes depolymerization of aggregates by monomer addition and dissociation reactions and does not consider fragmentation of aggregates into two oligomers. Involvement of these fragmentation reactions would result in much faster depolymerization kinetics and hence lower values of t-90. Hence, the qualitative kinetic model presented here correctly predicts a minimum depolymerization rate at the critical chloroform volume fraction, however, does not capture the full complexity of the depolymerization kinetics because fragmentation of one-dimensional aggregates is not taken into account. It should be mentioned that involvement of oligomer reactions or fragmentation in the depolymerization process has no influence on the thermodynamic analysis. Even though the equilibrium model describes the polymerization by sequentially monomer association and dissociation, also oligomer reactions and fragmentation are implicitly taken into account due to the principle of detailed balance.

The resemblance between the minimum protein (un)folding rate at the midpoint of the denaturation curve and the minimum disassembly rate at f_{crit} is remarkable, because of the differences in noncovalent interactions involved (dipolar vs hydrogen bonding), reaction order (intermolecular vs intramolecular), and solvent conditions (nonaqueous vs aqueous). To further analyze this phenomenon, we assess the influence of the

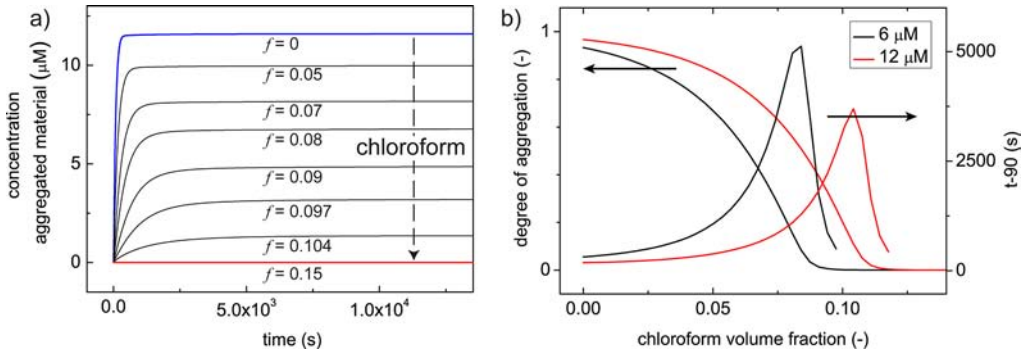

Figure 6. (a) The aggregation kinetics are simulated via the kinetic nucleation−elongation model, starting from only free monomers in different chloroform/MCH ratios (OPV dimer concentration 12 μM). In agreement with the depolymerization simulations, the rate constants depend on the chloroform volume fraction as described in eqs 2−4. (b) The time at which 90% of the conversion toward the equilibrium state is obtained (t-90) shows a minimum polymerization rate around the critical chloroform volume fraction ($a^0 = 6 \times 10^4\ M^{-1}s^{-1}$, $c^0 = 1.71 \times 10^{-2}\ s^{-1}$, $m_a = 7$, $m_c = 7$, $\sigma = 0.16$, $n = 5$).

cooperativity in the growth of the aggregates by simulations with the kinetic model. Interestingly, if cooperative effects are diminished ($\sigma \rightarrow 1$), the minimum depolymerization rate appears at lower values of f, and in case of isodesmic growth ($\sigma = 1$), the rate continuously increases with f. This demonstrates that cooperativity is a key parameter in observing the chevron-type depolymerization kinetics (Figure S12, Supporting Information).[25]

The minimum disassembly rate of a cooperative supramolecular polymer observed around the critical chloroform volume fraction can be rationalized by the influence of solvent composition on the length distribution. Upon increasing the fraction of good solvent (f), the equilibrium concentration of long stacks decreases, whereas the concentration of short stacks, (prenucleus) oligomers and monomers increases (Figure 5, Figure S13, Supporting Information). As a consequence, addition of free monomers in chloroform to a solution of long stacks in pure MCH results in two effects which occur simultaneously: (1) depolymerization of long aggregates to their new (shorter) equilibrium length as a consequence of the increased chloroform/MCH ratio; and (2) assembly of new monomers, either originating from the chloroform phase or from depolymerization of long stacks, into new oligomers and short aggregates. The first effect becomes stronger upon increasing f, either as a result of an increasing backward rate constant c or due to the decreasing forward rate constant a, both hampering elongation of long stacks. However, the same influence of chloroform on the rate constants deactivates the second effect, thereby slowing down the formation of new oligomers and short aggregates upon increasing f. Since the concentration of short aggregates and oligomers is negligible beyond f_{crit}, the first effect dominates the depolymerization rate in the regime $f > f_{crit}$, resulting in a rate that increases with the fraction of good solvent in this regime. However, in the regime $f < f_{crit}$, the monomers resulting from the depolymerization of long stacks aggregate into new short stacks (Figure S13, Supporting Information). This formation of short aggregates is slowed down upon increasing the chloroform volume fraction, both due to the decreasing forward rate constant a as well as the increasing backward rate constants b (nucleation) and c (elongation). For a cooperative supramolecular polymerization in which a nucleation step is involved in the formation of new aggregates, this results in a minimum equilibration rate at the critical chloroform volume fraction.

Next, the influence of solvent composition on the aggregation kinetics is investigated by simulating the build-up of aggregates starting from a solution of free monomers. Again, an important influence of nucleation is encountered (Figure S15, Supporting Information). Only for small values of σ, a minimum aggregation rate is observed at f_{crit} (Figure 6). In analogy to the influence of nucleation on the equilibration of OPV assemblies upon addition of chloroform, this phenomenon can be rationalized by the fact that for polymerization kinetics the rate of equilibration is determined by (1) the amount of material that is aggregated under equilibrium conditions and (2) the formation rate of new aggregates. Both the amount of material that aggregates under equilibrium conditions as well as the formation rate decrease with f. In case of cooperative growth, the nucleation of new aggregates, which is hampered upon increasing f, dominates the process. As a result, the simulated polymerization rate for cooperative systems decreases up to f_{crit}.

To further extend the insights from the kinetic model, we perform simulations on the aggregation kinetics in which the dependence of the forward and backward rate constants on the solvent composition is varied. In general, the thermodynamic stability of the assemblies as a function of chloroform volume fraction, f, is determined by the value of m in eq 1, with $m > 0$. On the other hand, the stability of the assemblies can be represented by the equilibrium constant of elongation $K_e = a/c$, in which the dependence of rate constants a and c on f is determined via m_a and m_c, respectively (eqs 2 and 3). Combining these two relations, it can be derived that K_e decreases with f if $m_a + m_c > 0$.[26] Hence, depolymerization upon addition of chloroform occurs when both rate constants increase with f, when both rate constants decrease with f and all possibilities in between, as long as the requirement $m_a + m_c > 0$ is met (Figure 7). The kinetic polymerization simulations show that if rate constants a and c are both decreasing functions with respect to f, a minimum polymerization rate is obtained at f_{crit} as a result of the decreasing rate of monomer association. If rate constant a decreases with respect to f and rate constant c increases is with f, also the increasing rate of monomer dissociation slows down the polymerization toward f_{crit}. However, if rate constant a increases with f, an interesting dependence of t-90 on solvent composition can be observed. Initially, the polymerization rate increases with f, and subsequently slows down toward f_{crit}. Apparently, for low values of f the increasing a dominates the polymerization rate, whereas close to f_{crit} the increasing c is dominant and slows down the polymerization. In analogy to this behavior, comparable results are obtained in simulations on depolymerization kinetics (Figure S16, Supporting Information). This indicates that, independent of the actual influence of solvent composition on

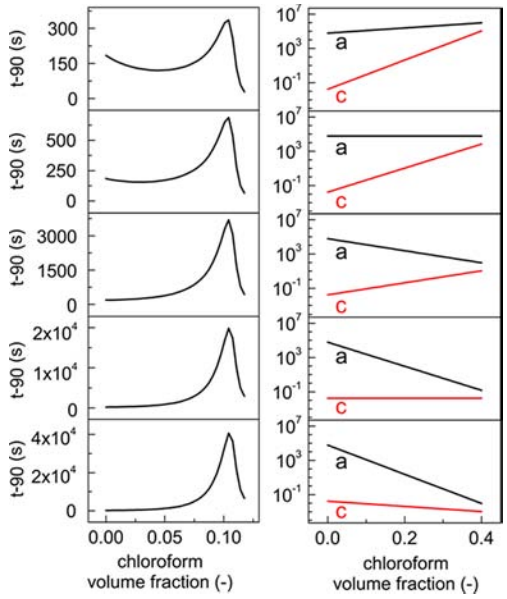

Figure 7. Aggregation kinetics simulated with the kinetic nucleation–elongation model show that if the slope of backward rate constant c as a function of f is less negative compared to the slope of forward rate constant a ($m_a + m_c > 0$), the minimum polymerization rate is obtained close to the critical solvent composition. The left pane shows the dependence of t-90 on f for the different relations between rate constants and solvent composition that are shown in the right pane. From top to bottom: $m_a = -3$, $m_c = 17$; $m_a = 0$, $m_c = 14$; $m_a = 7$, $m_c = 7$; $m_a = 14$, $m_c = 0$; $m_a = 17$, $m_c = -3$; rate constants are based on eqs 2–4, $a^0 = 6 \times 10^4$ $M^{-1}s^{-1}$, $c^0 = 1.71 \times 10^{-2}$ s^{-1}, $\sigma = 0.16$, $n = 5$, OPV dimer concentration 12 μM.

the forward and backward rate constants, addition of destabilizing cosolvent results in a slowing down of the rate of both assembly as well as disassembly close to the critical solvent composition.

3. CONCLUSIONS

The present study shows the influence of solvent conditions on the stability and dynamics of a supramolecular polymer. In analogy to protein denaturation models and studies on the unfolding of synthetic foldamers, addition of a cosolvent that weakly associates with the monomer (thereby acting as a "good" solvent) results in a linear decrease of the Gibbs free energy for monomer addition. The resulting depolymerization process reveals a critical solvent composition for supramolecular polymers that assemble via a cooperative mechanism, whereas a gradual disassembly profile is observed for supramolecular polymers that grow via an isodesmic mechanism.

The depolymerization experiments reveal a minimum rate of OPV disassembly close to the critical volume fraction of the good solvent. Because of the solvent-dependent dynamics, the mixing protocol applied to induce depolymerization is shown to have important consequences for the time-dependent development of the supramolecular polymers. Insufficient mixing can initially result in a (fast) depolymerization in one part of the solution, whereas in the final obtained homogeneous solution supramolecular polymerization is again initiated. The time scale of its assembly[9] and disassembly, which is in the order of 5–30 min, makes OPV an ideal model system to study supramolecular polymerization mechanisms in detail. Analysis of the dynamics of the other systems studied in this work, **2**–**4**, have shown that it is too fast for reliable studies on the assembly and disassembly kinetics, meaning that their assembly can only be studied under equilibrium conditions. However, the experimental results on OPV disassembly provide us general insights, as evidenced by the kinetic model developed in this paper. By taking into account the influence of solvent on the rate constants, the model captures the experimentally observed behavior and predicts a minimum disassembly rate at the critical solvent composition as well. By simulating the solvent-dependent kinetics using this model, we trace the origin of the slowest dynamics (both in polymerization and depolymerization) at the critical good/poor solvent ratio observed in cooperative systems back to the nucleation of new assemblies.

The observed relations between solvent composition and time-dependent development of a self-assembled system are envisioned to have important consequences for the formation of functional supramolecular systems. Previously it has been shown that the development of one-dimensional self-assemblies can be performed via a fast process by rapid dispersion of molecules into a poor solvent. However, if the association is too strong (e.g., due to strong interactions between the side chains), this methodology produces large agglomerates that precipitate.[6a] To slow down the assembly process, the mixing of good and poor solvent can be retarded via phase transfer[6a,27] (using a nonmiscible combination of good and poor solvent) or vapor diffusion.[28] However, the current study shows that the self-assembly rate can be further controlled by the ratio between good and poor solvent as well. This finding expands the toolbox to control the formation of one-dimensional nanomaterials across multiple length and time scales.

Moreover, in the stepwise assembly of multicomponent structures, a critical aspect that needs to be achieved is the exclusive growth of a new molecular building block on previously formed assemblies without nucleation of the new material. The most convenient way to achieve this is by addition of a new component in a good solvent to a solution containing aggregates in such a way that the new component cannot form new nuclei de novo. However, unless the assemblies formed in previous steps are locked by covalent fixation,[29] extremely strong noncovalent interactions, such as metal-ion binding[30] or crystallization,[31] the addition of a good solvent affects their stability as well. These factors complicate the design of multistep noncovalent syntheses. For example, the highly nonlinear relation between dynamics and solvent composition can, in case of an inhomogeneous addition of good solvent, result in a disassembly overshoot of the initially formed architectures. Only by understanding the influence of good and poor solvents on the thermodynamics and kinetics of self-assembly processes, optimized noncovalent synthetic strategies can be developed which will pave the way toward functional multicomponent supramolecular systems.

4. EXPERIMENTAL AND COMPUTATIONAL SECTION

The syntheses and molecular characterizations of molecules **1**–**4** are described or will be described elsewhere.[13−16] The denaturation experiments are performed by adding solutions of the monomer in chloroform (good solvent) in different amounts to solutions of the aggregates in MCH. The disassembly is probed by CD (**1**, 466 nm; **2**, 316 nm; **3**, 286 nm) or UV–vis (**4**, at maximum intensity ranging from 518–528 nm) spectroscopy under equilibrium conditions verified by time-dependent experiments. Data are analyzed via a global nonlinear least-squares curve-fitting method using the equilibrium model with Gibbs free energy of monomer association linearly dependent on the chloroform volume fraction. In the global optimization routine, a local optimization solver (Matlab, lsqnonlin solver) is supplied with a range of

initial values generated using a quasi-random number generator (Matlab, lhsdesign). This ensures that the basins of attraction of all local minima are uniformly sampled resulting in the global minimum of the cost function. The time at which 90% of the conversion toward the equilibrium state is obtained (t-90) is determined by the time t at which $(CD_0 - CD(t))/(CD_0 - CD_{steady\ state}) = 0.90$. In this equation, $CD_{steady\ state}$ represents the final CD-value, $CD(t)$ the CD-value at time t, and CD_0 the initial CD-value in pure MCH corrected for dilution with the chloroform phase (i.e., $CD_0 = CD_{MCH} \cdot (1 - f)$). The kinetic model describes the reversible assembly and disassembly of a supramolecular polymer as a sequence of monomer association and dissociation reactions. For each species with length i, the time-dependent development of concentration is described via a differential equation. To limit the amount of differential equations required to describe the kinetics, it is assumed that for $i > N$, with $N \gg n$ ($N = 100$) $[X_{i+1}] = \alpha[X_i]$, as introduced in ref 9. The resulting system of $N + 2$ differential equations is solved in Matlab (ode15s solver).

■ ASSOCIATED CONTENT

Supporting Information

Additional spectroscopic data, temperature-dependent assembly curves, details on the equilibrium model, details on the curve-fitting procedure and results thereof, kinetic stopped-flow data of OPV depolymerization, details on the kinetic model, and depolymerization and polymerization kinetics simulations. This material is available free of charge via the Internet at http://pubs.acs.org.

■ AUTHOR INFORMATION

Corresponding Author

t.f.a.d.greef@tue.nl; e.w.meijer@tue.nl

Notes

The authors declare no competing financial interest.

■ ACKNOWLEDGMENTS

We like to thank Dr. Christophe Grenier, Dr. Subi J. George, Dr. Tristan Mes, Dr. Floris A. Helmich, and Dr. Anja R. A. Palmans, Eindhoven University of Technology, for providing samples of the molecules and fruitful discussions. The research leading to these results has received funding from the European Research Council under the European Union's Seventh Framework Programme (FP/2007-2013)/ERC grant agreement number 246829 and from The Netherlands Organization for Scientific Research.

■ REFERENCES

(1) (a) Service, R. F. *Science* **2005**, *309*, 95. (b) Lehn, J.-M. *Angew. Chem., Int. Ed.* **1990**, *29*, 1304−1319. (c) Whitesides, G. M.; Grzybowski, B. *Science* **2002**, *295*, 2418−2421. (d) Grzybowski, B. A.; Wilmer, C. E.; Kim, J.; Browne, K. P.; Bishop, K. J. M. *Soft Matter* **2009**, *5*, 1110−1128. (e) Rybtchinski, B. *ACS Nano* **2011**, *5*, 6791−6818.

(2) Some selected examples: (a) Bong, D. T.; Clark, T. D.; Granja, J. R.; Ghadiri, M. R. *Angew. Chem., Int. Ed.* **2001**, *40*, 988−1011. (b) Birchall, L. S.; Roy, S.; Jayawarna, V.; Hughes, M.; Irvine, E.; Okorogheye, G. T.; Saudi, N.; De Santis, E.; Tuttle, T.; Edwards, A. A.; Ulijn, R. V. *Chem. Sci.* **2011**, *2*, 1349−1355. (c) Carnall, J. M. A.; Waudby, C. A.; Balenguer, A. M.; Stuart, M. C. A.; Peyralans, J. J.-P.; Otto, S. *Science* **2010**, *327*, 502−506. (d) Coleman, A. C.; Beierle, J. M.; Stuart, M. C. A.; Maciá, B.; Caroli, G.; Mika, J. T.; van Dijken, D. J.; Chen, J.; Browne, W. R.; Feringa, B. L. *Nat. Nanotechnol.* **2011**, *6*, 547−552. (e) Estroff, L. A.; Hamilton, A. D. *Chem. Rev.* **2004**, *104*, 1201. (f) Yan, Y.; Lin, Y.; Qiao, Y.; Huang, J. *Soft Matter* **2011**, *7*, 6385−6398. (g) Adamcik, J.; Castelletto, V.; Bolisetty, S.; Hamley, I. W.; Mezzenga, R. *Angew. Chem., Int. Ed.* **2011**, *50*, 5495−5498. (h) Kim, S. H.; Nederberg, F.; Jakobs, R.; Tan, J. P. K.; Fukushima, K.; Nelson, A.; Meijer, E. W.; Yang, Y. Y.; Hedrick, J. L. *Angew. Chem., Int. Ed.* **2009**, *48*, 4508−4512. (i) van Hameren, R.; Schön, P.; van Buul, A. M.; Hoogboom, J.; Lazarenko, S. V.; Gerritsen, J. W.; Engelkamp, H.; Christianen, P. C. M.; Heus, H. A.; Maan, J. C.; Rasing, T.; Speller, S.; Rowan, A. E.; Elemans, J. A. A. W.; Nolte, R. J. M. *Science* **2006**, *314*, 1433−1436. (j) Gielen, J. C.; Ver Heyen, A.; Klyatskaya, S.; Vanderlinden, W.; Höger, S.; Maan, J. C.; De Feyter, S.; Christianen, P. C. M. *J. Am. Chem. Soc.* **2009**, *131*, 14134−14135.

(3) (a) Hoeben, F. J. M.; Jonkheijm, P.; Meijer, E. W.; Schenning, A. P. H. J. *Chem. Rev.* **2005**, *105*, 1491−1546. (b) Chen, Z.; Lohr, A.; Saha-Möller, C. R.; Würthner, F. *Chem. Soc. Rev.* **2009**, *38*, 564−584. (c) Shao, H.; Seifert, J.; Romano, N. C.; Gao, M.; Helmus, J. J.; Jaroniec, C. P.; Modarelli, D. A.; Parquette, J. R. *Angew. Chem., Int. Ed.* **2010**, *49*, 1−5. (d) Liao, Q.; Fu, H.; Wang, C.; Yao, J. *Angew. Chem., Int. Ed.* **2011**, *50*, 4942−4946. (e) Sheng, Y.; Fu, H.; Peng, A.; Ma, Y.; Liao, Q.; Yao, J. *Acc. Chem. Res.* **2010**, *43*, 409−418. (f) Hasegawa, M.; Iyoda, M. *Chem. Soc. Rev.* **2010**, *39*, 2420−2427. (g) Chaudhuri, D.; Li, D.; Che, Y.; Shafran, E.; Gerton, J. M.; Zang, L.; Lupton, J. M. *Nano Lett.* **2011**, *11*, 488−492. (h) Zhang, C.; Zou, C.-L.; Yan, Y.; Hao, R.; Sun, F.-W.; Han, Z.-F.; Zhao, Y. S.; Yao, J. *J. Am. Chem. Soc.* **2011**, *133*, 7276−7279. (i) Kim., F. S.; Ren, G.; Jenekhe, S. A. *Chem. Mater.* **2011**, *23*, 682−732. (j) Nussbaumer, A. L.; Studer, D.; Malinovskii, V. L.; Häner, R. *Angew. Chem., Int. Ed.* **2011**, *50*, 5490−5494. (k) Neelakandan, P. P.; Pan, Z.; Hariharan, M.; Zheng, Y.; Weissman, H.; Rybtchinski, B.; Lewis, F. D. *J. Am. Chem. Soc.* **2010**, *132*, 15808−15813. (k) Bullock, J. E.; Carmieli, R.; Mickley, S. M.; Vura-Weis, J.; Wasielewski, M. R. *J. Am. Chem. Soc.* **2009**, *131*, 11919−11929. (l) Rancatore, B. J.; Mauldin, C. E.; Tung, S.-H.; Wang, C.; Hexemer, A.; Strzalka, J.; Fréchet, J. M. J.; Xu, T. *ACS Nano* **2010**, *5*, 2721−2729.

(4) (a) Capito, R. M.; Azevedo, H. S.; Velichko, Y. S.; Mata, A.; Stupp, S. I. *Science* **2008**, *319*, 1812−1816. (b) Palmer, L. C.; Stupp, S. I. *Acc. Chem. Res.* **2008**, *41*, 1674−1684. (c) Dankers, P. Y. W.; Harmsen, M. C.; Brouwer, L. A.; Van Luyn, M. J. A.; Meijer, E. W. *Nat. Mater.* **2005**, *4*, 568−574. (d) Tsang, B. P.; Bretscher, H. S.; Kokona, B.; Manning, R. S.; Fairman, R. *Biochemistry* **2011**, *50*, 8548−8558. (e) Müller, M. K.; Brunsveld, L. *Angew. Chem., Int. Ed.* **2009**, *48*, 2921−2924.

(5) Aida, T.; Meijer, E. W.; Stupp, S. I. *Science* **2012**, *335*, 813−817.

(6) (a) Zhang, L.; Che, Y.; Moore, J. S. *Acc. Chem. Res.* **2008**, *41*, 1596−1608. (b) Oh, J. H.; Lee, H. W.; Mannsfeld, S.; Stoltenberg, R. M.; Jung, E.; Jin, Y. W.; Kim, J. M.; Yoo, J.-B.; Bao, Z. *Proc. Natl. Acad. Sci. U.S.A.* **2009**, *106*, 6065−6070. (c) Zhao, Y. S.; Fu, H.; Peng, A.; Ma, Y.; Liao, Q.; Yao, J. *Acc. Chem. Res.* **2010**, *43*, 409−418. (d) Kim, D. H.; Lee, D. Y.; Lee, H. S.; Lee, W. H.; Kim, Y. H.; Han, J. I.; Cho, K. *Adv. Mater.* **2007**, *19*, 678−682. (e) Briseno, A. L.; Mannsfeld, S. C. B.; Reese, C.; Hancock, J. M.; Xiong, Y.; Jenekhe, S. A.; Bao, Z.; Xia, Y. *Nano Lett.* **2007**, *7*, 2847−2853. (f) Balakrishnan, K.; Datar, A.; Oitker, R.; Chen, H.; Zuo, J.; Zang, L. *J. Am. Chem. Soc.* **2005**, *127*, 10496−10497. (g) Che, Y.; Datar, A.; Balakrishnan, K.; Zang, L. *J. Am. Chem. Soc.* **2007**, *129*, 7234−7235. (h) Yamamoto, Y.; Fukushima, T.; Suna, Y.; Ishii, N.; Saeki, A.; Seki, S.; Tagawa, S.; Taniguchi, M.; Kawai, T.; Aida, T. *Science* **2006**, *314*, 1761−1764. (i) Zhang, C.; Zou, C.-L.; Yan, Y.; Hao, R.; Sun, F.-W.; Han, Z.-F.; Zhao, Y. S.; Yao, J. *J. Am. Chem. Soc.* **2011**, *133*, 7276−7279. (j) Abbel, R.; Van Der Weegen, R.; Meijer, E. W.; Schenning, A. P. H. J. *Chem. Commun.* **2009**, 1697−1699. (k) Enozawa, H.; Hasegawa, M.; Takamatsu, D.; Fukui, K.; Iyoda, M. *Org. Lett.* **2006**, *8*, 1917−1920. (l) Percec, V.; Wilson, D. A.; Leowanawat, P.; Wilson, C. J.; Hughes, A. D.; Kaucher, M. S.; Hammer, D. A.; Levine, D. H.; Kim, A. J.; Bates, F. S.; Davis, K. P.; Lodge, T. P.; Klein, M. L.; DeVane, R. H.; Aqad, E.; Rosen, B. M.; Argintaru, A. O.; Sienkowska, M. J.; Rissanen, K.; Nummelin, S.; Ropponen, J. *Science* **2010**, *328*, 1009−1014. (m) Kim, K. T.; Zhu, J.; Meeuwissen, S. A.; Cornelissen, J. J. L. M.; Pochan, D. J.; Nolte, R. J. M.; Van Hest, J. C. M. *J. Am. Chem. Soc.* **2010**, *132*, 12522−12524. (p) Cui, H.; Chen, Z.; Zhong, S.; Wooley, K. L.; Pochan, D. J. *Science* **2007**, *317*, 647−650.

(7) (a) Mes, T.; Smulders, M. M. J.; Palmans, A. R. A.; Meijer, E. W. *Macromolecules* **2010**, *43*, 1981−1991. (b) Mammen, M.; Simanek, E. E.; Whitesides, G. M. *J. Am. Chem. Soc.* **1996**, *118*, 12614−12623. (c) Bouteillier, L.; van der Schoot, P. *J. Am. Chem. Soc.* **2012**, *134*, 1363−1366. (d) Kastler, M.; Pisula, W.; Wasserfallen, D.; Pakula, T.; Müllen, K. *J. Am. Chem. Soc.* **2005**, *127*, 4286−4296. (e) Tobe, Y.; Utsumi, N.;

Kawabata, K.; Nagano, A.; Adachi, K.; Araki, S.; Sonoda, M.; Hirose, K.; Naemura, K. *J. Am. Chem. Soc.* **2002**, *124*, 5350−5364. (f) Castellano, R. K.; Clark, R.; Craig, S. L.; Nuckolls, C.; Rebek, J., Jr. *Proc. Natl. Acad. Sci. U.S.A.* **2000**, *97*, 12418−12421. (g) Cook, J. L.; Hunter, C. A.; Low, C. M. R.; Perez-Velasco, A.; Vinter, J. G. *Angew. Chem., Int. Ed.* **2007**, *46*, 3706−3709. (h) Ponnuswamy, N.; Pantoş, G. D.; Smulders, M. M. J.; Sanders, J. K. M. *J. Am. Chem. Soc.* **2012**, *134*, 566−573. (i) Nieuwenhuizen, M. M. L.; de Greef, T. F. A.; van der Bruggen, R. L. J.; Paulusse, J. M. J.; Appel, W. P. J.; Smulders, M. M. J.; Sijbesma, R. P.; Meijer, E. W. *Chem.—Eur. J.* **2010**, *16*, 1601−1612. (j) Besenius, P; van den Hout, K. P.; Albers, H. M. H. G.; de Greef, T. F. A.; Olijve, L. L. C.; Hermans, T. M.; de Waal, B. F. M.; Bomans, P. H. H.; Sommerdijk, N. A. J. M.; Portale, G.; Palmans, A. R. A.; van Genderen, M. H. P.; Vekemans, J. A. J. M.; Meijer, E. W. *Chem.—Eur. J.* **2011**, *17*, 5193−5203. (k) Görl, D.; Zhang, X.; Würthner, F. *Angew. Chem., Int. Ed.* **2012**, *51*, 2−23. (l) Corbin, P. S.; Lawlessa, L. J.; Li, Z.; Ma, Y.; Witmer, M. J.; Zimmerman, S. C. *Proc. Natl. Acad. Sci. U.S.A.* **2002**, *99*, 5099−5104.

(8) (a) Boekhoven, J.; Brizard, A. M.; van Rijn, P.; Stuart, M. C. A.; Eelkema, R.; Van Esch, J. H. *Angew. Chem., Int. Ed.* **2011**, *50*, 12285−12289. (b) Obert, E.; Bellot, M.; Bouteiller, L.; Andrioletti, F.; Lehen-Ferrenbach, C.; Boué, F. *J. Am. Chem. Soc.* **2007**, *129*, 15601−15605. (c) Dasgupta, D.; Srinivasan, S.; Rochas, C.; Ajayashosh, A.; Guenet, J.-M. *Soft Matter* **2011**, *7*, 9311−9315. (d) Bouteiller, L.; Colombani, O.; Lortie, F.; Terech, P. *J. Am. Chem. Soc.* **2005**, *127*, 8893−8898. (d) Tidhar, Y.; Weissman, H.; Wolf, S. G.; Gulino, A.; Rybtchinski, B. *Chem.—Eur. J.* **2011**, *17*, 6068−6075. (e) Canevet, D.; Pérez del Pino, Á.; Amabilino, D. B.; Sallé, M. *J. Mater. Chem.* **2011**, *21*, 1428−1437.

(9) Korevaar, P. A.; George, S. J.; Markvoort, A. J.; Smulders, M. M. J.; Hilbers, P. A. J.; Schenning, A. P. H. J.; de Greef, T. F. A.; Meijer, E. W. *Nature* **2012**, *481*, 492−496.

(10) England, J. L.; Haran, G. *Annu. Rev. Phys. Chem.* **2011**, *62*, 257−277.

(11) (a) Tanford, C. *J. Am. Chem. Soc.* **1964**, *86*, 2050−2059. (b) Scholtz, J. M.; Grimsley, G. R.; Pace, C. N. *Methods Enzymol.* **2009**, *466*, 549−565. (c) Greene, R. F.; Pace, C. N. *J. Biol. Chem.* **1974**, *249*, 5388−5393.

(12) (a) Tanford, C. *Adv. Protein Chem.* **1968**, *23*, 121−282. (b) Matthews, C. R. *Methods Enzymol.* **1987**, *154*, 498−511. (c) Liu, Z.; Reddy, G.; O'Brien, E. P.; Thirumalai, D. *Proc. Natl. Acad. Sci. U.S.A.* **2011**, *108*, 7787−7792.

(13) The synthesis of **1** will be published soon, but the synthesis and properties of the (*S*)-enantiomer are reported in detail: Schenning, A. P. H. J.; Jonkheijm, P.; Peeters, E.; Meijer, E. W. *J. Am. Chem. Soc.* **2001**, *123*, 409−416.

(14) The synthesis and properties of **2** will be published elsewhere, but the carbonyl structures are all published in detail: (a) Brunsveld, L.; Schenning, A. P. H. J.; Broeren, M. A. C.; Janssen, H. M.; Vekemans, J. A. J. M.; Meijer, E. W. *Chem. Lett.* **2000**, 292−293. (b) Stals, P. J. M.; Smulders, M. M. J.; Martín-Rapún, R.; Palmans, A. R. A.; Meijer, E. W. *Chem.—Eur. J.* **2009**, *15*, 2071−2080.

(15) Palmans, A. R. A.; Vekemans, J. A. J. M.; Havinga, E. E.; Meijer, E. W. *Angew. Chem., Int. Ed.* **1997**, *36*, 2648−2651.

(16) Chen, Z.; Stepanenko, V.; Volker, D.; Prins, P.; Siebbeles, L. D. A.; Seibt, J.; Marquetand, P.; Engel, V.; Würthner, F. *Chem.—Eur. J.* **2007**, *13*, 436−449.

(17) (a) Smulders, M. M. J.; Nieuwenhuizen, M. M. L.; de Greef, T. F. A.; van der Schoot, P.; Schenning, A. P. H. J.; Meijer, E. W. *Chem.—Eur. J.* **2010**, *16*, 362. (b) de Greef, T. F. A.; Smulders, M. M. J.; Wolffs, M.; Schenning, A. P. H. J.; Sijbesma, R. P.; Meijer, E. W. *Chem. Rev.* **2009**, *109*, 5687. (c) Zhao, D.; Moore, J. S. *Org. Biomol. Chem.* **2003**, *1*, 3471−3491.

(18) Jonkheijm., P.; van der Schoot, P.; Schenning, A. P. H. J.; Meijer, E. W. *Science* **2006**, *313*, 80−83.

(19) Metzroth, T.; Hoffmann, A.; Martín-Rapún, R.; Smulders, M. M. J.; Pieterse, K.; Palmans, A. R. A.; Vekemans, J. A. J. M.; Meijer, E. W.; Spiess, H. W.; Gauss, J. *Chem. Sci.* **2011**, *2*, 69−76.

(20) Goldstein, R. F.; Stryer, L. *Biophys. J.* **1986**, *50*, 583−599.

(21) (a) Schellman, J. A. *Biopolymers* **1975**, *14*, 999. (b) Schellman, J. A. *Biophys. Chem.* **2002**, *96*, 91. (c) Auton, M.; Holthauzen, L. M. F.; Bolen, D. W. *Proc. Natl. Acad. Sci. U.S.A.* **2007**, *104*, 15317−15322.

(22) Prince, R. B.; Saven, J. G.; Wolynes, P. G.; Moore, J. S. *J. Am. Chem. Soc.* **1999**, *121*, 3114−3121.

(23) Alternatively, an overshoot in depolymerization can be explained by the fact that the curve which represents the degree of aggregation under equilibrium conditions as a function of f exceeds the initial degree of aggregation obtained upon homogeneous mixing, which is on the line $y = 1 - f$. However, as shown in Figure S6, Supporting Information, at this concentration this is not the case.

(24) In this supramolecular polymerization model, the hydrogen-bonded OPV dimer is considered as the building-block (i.e., monomer) in the aggregation process. In the kinetic model introduced in ref 9, two assembly pathways are taken into account to describe the polymerization process: a kinetically vs thermodynamically controlled pathway that are competing for the same free monomer. In the analysis followed in this paper however, only one assembly pathway towards the thermodynamically stable aggregate is considered. This simplification is justified because of the limited influence of the kinetic assembly pathway in the simulation of depolymerization kinetics, as shown in Figure S11, Supporting Information. Moreover, this simplification extends the applicability of the simulations to other supramolecular systems.

(25) Also if the addition of pure chloroform, rather than OPV monomers in chloroform, to OPV assemblies in MCH is simulated, a minimum depolymerization rate at f_{crit} is observed for cooperative systems (Figure S14, Supporting Information).

(26) As follows from eq 1, $\Delta G^{0\prime}$ increases with f if $m > 0$, resulting in a decrease of K_e with f. Alternatively, K_e can be found via $\log(K_e) = \log(a/c) = \log(a^0/c^0) - (m_a + m_c)f = \log(K_e^0) - (m_a + m_c)f$, $\ln(K_e) = \ln(K_e^0) - 2.3026(m_a + m_c)f$. Subsequently expressing K_e and K_e^0 in $\Delta G^{0\prime}$ and ΔG^0, respectively, yields: $\Delta G^{0\prime} = \Delta G^0 + 2.3026 \cdot RT(m_a + m_c)f$. As a result, m equals $2.3026 \cdot RT\ (m_a + m_c)$ and $m_a + m_c > 0$ if $m > 0$.

(27) Balakrishnan, K.; Datar, A.; Naddo, T.; Huang, J.; Oitker, R.; Yen, M.; Zhao, J.; Zang., L. *J. Am. Chem. Soc.* **2006**, *128*, 7390−7398.

(28) (a) Che, Y.; Zang, X.; Loser, S.; Zang, L. *Nano Lett.* **2008**, *8*, 2219−2223. (b) Wang, S.; Dössel, L.; Mavrinskiy, A.; Gao, P.; Feng, X.; Pisula, W.; Müllen, K. *Small* **2011**, *7*, 2841−2846. (c) Xu, G.; Tang, Y.-B.; Tsang, C.-H.; Zapien, J.-A.; Lee, C.-S.; Wong, N.-B. *J. Mater. Chem.* **2010**, *20*, 3006−3010.

(29) (a) Grill, L.; Dyer, M.; Lafferentz, L.; Persson, M.; Peters, M. V.; Hecht, S. *Nat. Nanotechnol.* **2007**, *2*, 687−691. (b) Fujita, N.; Sakamoto, Y.; Shirakawa, M.; Ojima, M.; Fujii, A.; Ozaki, M.; Shinkai, S. *J. Am. Chem. Soc.* **2007**, *129*, 4134−4135. (c) Dautel, O. J.; Robitzer, M.; Lère-Porte, J.-P.; Serein-Spirau, F.; Moreau, J. J. E. *J. Am. Chem. Soc.* **2006**, *128*, 16213−16223.

(30) Zhang, W.; Jin, W.; Fukushima, T.; Saeki, A.; Seki, S.; Aida, T. *Science* **2011**, *334*, 340−343.

(31) (a) Wang, X.; Guerin, G.; Wang, H.; Wang, Y.; Manners, I.; Winnik, M. A. *Science* **2007**, *317*, 644−647. (b) Gilroy, J. B.; Gädt, T.; Whittell, G. R.; Chabanne, L.; Mitchels, J. M.; Richardson, R. M.; Winnik, M. A.; Manners, I. *Nature Chem.* **2010**, *2*, 566−570. (c) Zheng, J. Y.; Yan, Y.; Wang, X.; Zhao, Y. S.; Huang, J.; Yao, J. *J. Am. Chem. Soc.* **2012**, *134*, 2880−2883.

NOTE ADDED AFTER ASAP PUBLICATION

Due to a production error, this paper was published on the Web on August 2, 2012, with minor text errors. The wavelengths used for the CD study of **1**, **2**, and **3** were clarified in the first paragraph of section 4, and the expression for $\Delta G^{0\prime}$ in ref 26 was corrected. The corrected version was reposted on August 3, 2012.